IEEE Access
Multidisciplinary | Rapid Review | Open Access Journal

Received 31 January 2023, accepted 14 February 2023, date of publication 23 February 2023, date of current version 1 March 2023.

Digital Object Identifier 10.1109/ACCESS.2023.3248238

RESEARCH ARTICLE

Interactive Visual Inspection of a Rough-Alignment Plastic Part Based on HLAC Features and One-Class SVM

TAIGA EGUCHI, WEN LIANG YEOH, HIROSHI OKUMURA, NOBUHIKO YAMAGUCHI, AND OSAMU FUKUDA, (Member, IEEE)

Department of Information Science, Graduate School of Science and Engineering, Saga University, Saga 840-8502, Japan

Corresponding author: Wen Liang Yeoh (wlyeoh@cc.saga-u.ac.jp)

This work was supported by the Adaptable and Seamless Technology Transfer Program through the Target-Driven Research and Development (A-STEP), Japan Science and Technology Agency (JST).

This work involved human subjects or animals in its research. Approval of all ethical and experimental procedures and protocols was granted by the Ethics Committee of the Faculty of Medicine at Saga University under Application No. R1-70.

ABSTRACT Modern production lines for molded plastic parts often have automated inspection systems to detect defective parts reliably and efficiently. However, these conventional inspection systems have low flexibility and versatility, leading to difficulties when dealing with complicated requests such as when small quantities of many different parts are manufactured on the same production line. The proposed system can be implemented quickly using low-cost off-the-shelf components and does not require accurate alignment of production parts, reducing the need for manual inspections and increasing work efficiency when handling complex workloads. The inspection algorithm combines higher-order local auto correlation (HLAC) features with one-class support vector machine (one-class SVM) and principal component analysis (PCA) to extract, transform, and classify the differential feature vector between conforming and nonconforming plastic parts. To verify its validity and effectiveness, we compared defect detection accuracy and speed between the developed inspection system and manual inspection experimentally. Extremely high accuracy (Recall = 0.93, Specificity = 1.00) and speed (10 inspections in 30[sec]) was obtained with 7 types (1 conforming type, 6 nonconforming types) of sample parts (30 samples each). We demonstrated a 400 % increase in speed can be gained relative to manual inspection.

INDEX TERMS Higher-order local auto-correlation feature, interactive, one-class support vector machine, plastic parts, rough alignment, visual inspection.

I. INTRODUCTION

In order to meet the continuous pressure to increase production, reduce costs, and improve quality, production facilities have to be able to inspect products as fast as possible. This is made more challenging by the increasing heterogeneity of products on production lines; wider array products are being produced in ever smaller quantities due to increasingly diverse consumer taste and demand for customized products. This has led to extremely high burdens on manufacturing staff as they attempt to cater to their customer's increasingly complex and diverse requests. For example, it often happens in actual production sites that different products are produced on the same production line in the mornings and afternoons, and sudden changes in the production schedule often occur. There is a need for an automatic image inspection system that is highly versatile and flexible that can handle wide ranges and variations of

The associate editor coordinating the review of this manuscript and approving it for publication was Antonio J. R. Neves.

plastic parts made from different production processes. This paper proposes an automatic inspection system that does not require accurate alignment of the plastic parts for it to work. By removing time-consuming alignment and preparation work, high-speed and high-accuracy automatic image-based defect inspection that is also easy to use can be realized.

When image-based defect inspection was first introduced on production lines, most inspection algorithms for detecting anomalies were using pixel-based or histogram-based image comparisons [1], or methods based on statistical features such as image texture [2]. However, precise alignment and controlled lighting conditions of the parts were necessary for these algorithms to be accurate. Achieving these inspection conditions required a lot of time, and placement and lighting conditions varied from product to product, limiting these algorithms' versatility and usefulness for multi-product lines. Our research group is also applying deep learning to detect black spots on components

With recent dramatic improvements in computing power, deep convolution neural networks composed of extremely large numbers of layers have been proposed and have been shown to have revolutionary high performance for image recognition [3], [4]. A feature of this method is that the models are trained in an end-to-end manner using large amounts of sample data, and specific features do not need to be manually determined for anomaly detection to be achieved.

For instance, the algorithms of YOLO [5] and AWS Rekognition [6] do not need alignment of the recognition target. In both these algorithms, the class recognition and position estimation of objects in the image are realized at the same time. Anomaly detection algorithms based on these deep learning models have the great advantage of being highly flexible and versatile, like human inspectors. However, deep learning models have a fatal disadvantage in that they require large amounts of sample data to train. Collecting anomalous data samples is extremely difficult, since they are rarely observed. Furthermore, the process of anomaly detection by these end-to-end methods becomes a black box, making it hard to backtrace and determine the reason why a part was deems to be anomalous by the model.

As will be explained in more detail in Section II, higher-order local auto-correlation (HLAC) [7] features refer to the integral values of local auto-correlations in the image. This can be obtained with relative ease using minimal calculations. One advantage of HLAC features is the shift invariance of its output. Additionally, the relatively simple calculation reduces computing load, which makes high-speed processing achievable, even without using a specialized computing unit, for example the GPU (Graphics Processing Unit). HLAC features have been applied to many studies thus far. In the medical field, HLAC feature was used for detecting bleeding and tumors from image data measured with a capsule endoscope [8], evaluate liver cirrhosis from an ultrasonic B-mode image [9], and extracting blood vessels from a retinal image [10]. Many researchers have also applied HLAC features to human motion analysis and man-machine interfaces (e.g. identification of gestures). For example, individual identification of gait movements and motion recognition of hand gestures have been attempted so far [11]. There have also been few applications in industrial production. There was a study [12], [13] that attempted to detect hot spots that caused defects at the pattern transfer to a semiconductor wafer. In [14], general objects were recognized from satellite image data.

Generally, training of a classifier requires large numbers of nonconforming samples, which can be difficult to acquire in practical applications due to the rarity of defective products. To solve the problem, we propose using a support vector machine (SVM) [15], which enables the model to be trained using only conforming samples. In one-class support vector machine (one-class SVM) [16], the model is trained only from conforming samples, and the outlier is detected as an nonconforming sample based on the trained model.

Similar discriminators include Isolation Forest [17], [18], Local Outlier Factor (LOF) [19], and Elliptic Envelope [20], which perform outlier detection using decision trees, density of the data distribution, and elliptical boundary of around a normal distribution, respectively. Isolation Forest assumes that the characteristics of conforming and nonconforming data are far apart. Therefore, it is considered unsuitable for detecting minute abnormalities such as those that occur at manufacturing sites. LOF is a robust discriminator for outlier detection, but it requires arbitrarily setting the number of points in the neighborhood of conforming data, and the definition of outliers is unclear. Therefore, while it is possible to detect outliers with conforming data only, it was difficult to set a threshold when classifying those with feature points in the neighborhood. This is because nearby points contain feature points of abnormality. Therefore, it is considered difficult to introduce LOF into a visual inspection system at a manufacturing site, where changes in minute abnormalities need to be detected. Finally, an Elliptic Envelope assumes that the data follows a normal distribution. One-class SVM was chosen because it does not have the disadvantages of the other discriminators mentioned and does not make assumptions of the distribution of the underlying data, allowing for a more flexible discriminant curve.

The primary objective of this paper is to clarify the effectiveness of the proposed HLAC features and their preprocessing. The chosen discriminator, One-class SVM, was compared to the Elliptic Envelope, which has a different decision boundary mechanism.

This study proposes a novel automatic image inspection algorithm that combines HLAC-based feature extraction and SVM classifier. The proposed method calculates the difference between the HLAC features extracted from the target plastic part and that of the reference conforming part, then transforms the principal axes of the feature space based on principal component analysis (PCA) [21] to enhance the

anomalous features of the target part. After transforming the principal axes, the extracted features are modeled using the SVM. Then, the model incorporates the normal variations in the features of the product, and the sample with outlier feature is detected as an nonconforming sample.

To make the best use of HLAC features, the effective preprocessing according to the target application is essential. However, if the HLAC features used without any preprocessing, high anomalous detection performance cannot be achieved. The performance can be maximized by optimizing the entire system (dynamic range and resolution of the image, preprocessing such as difference extraction and normalization, HLAC and SVM parameters). In the paper, we examine and report on the technologies, procedures, as well as the evaluation results achieved when applying HLAC features to anomaly inspection of plastic molded parts.

The paper is organized as follows: Section II explains the idea of the proposed method, and Section III shows the system configuration. Experiments conducted on the developed system and the results are presented in Section IV. We then draw some conclusions and outline the future work in Section V.

II. IDEA OF VISUAL INSPECTION OF A ROUGH-ALIGNMENT PLASTIC PART

The proposed defect inspection system has the following advantages.

- Highly efficient inspection without precise alignment of the parts
- Model training with only a small amount of conforming samples
- High-speed processing on a non-GPU computer
- Interactive inspection while monitoring the results in real time
- No need to collect defective samples

This section briefly explains the ideas of the algorithm.

A. MEASURING ENVIRONMENT AND INSPECTION TARGET

An overview of the image inspection system developed is shown in Fig. 1.

Unlike traditional defective inspection systems, where precise placement or alignment of plastic parts are required, our system allows the plastic parts to be placed roughly. In traditional systems, this requirement is achieved either using jigs or through software processing to compensate for misalignment. However, jigs can be difficult to replace or make on short notice, and expensive hardware and software that can detect and process minute changes is required to correct for misalignment. Our system removes this requirement by accounting for minor misalignment in our inspection model.

Furthermore, traditional systems often require a special environment such as a dark room to be effective. This is because small changes in brightness often occur, for example, due to people walking by or by the opening and closing doors. Our system also attempts to account for these variations, so it can be used in normal everyday lighting environments. This can substantially reduce the operational burden and improve the usability of the defect inspection system.

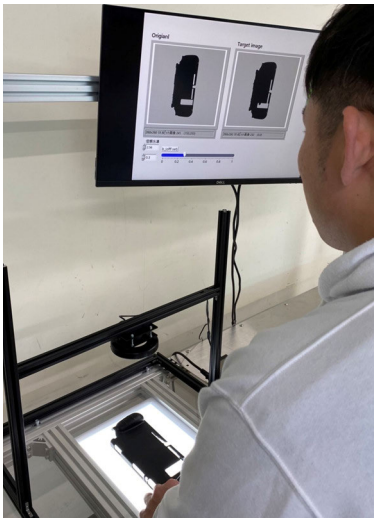

FIGURE 1. Overview of the visual inspection of a rough-alignment plastic part.

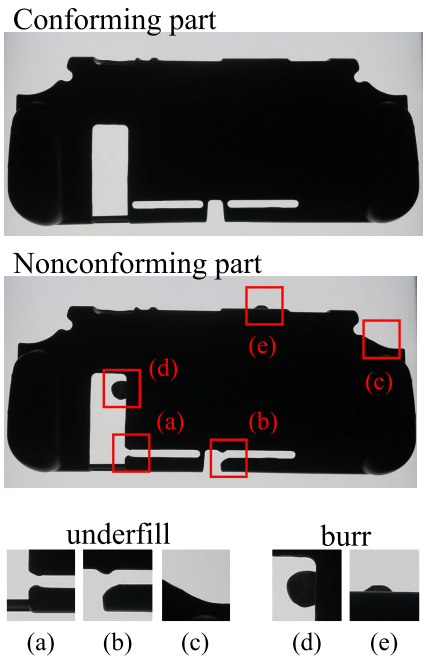

FIGURE 2. Example of the inspection target.

This study focuses on underfill and burr defects, which are typical in molded plastic parts. An example of a conforming and nonconforming part is shown in Fig. 2. These defects can be easily observed through a silhouette by illuminating the plastic part with a backlight. (a), (b), and (c) show the underfill defects, while (d) and (e) show the burr defects.

Although these kinds of defects may seem relatively easy to detect by a human inspector, they are also often overlooked when a large number of parts need to be inspected quickly.

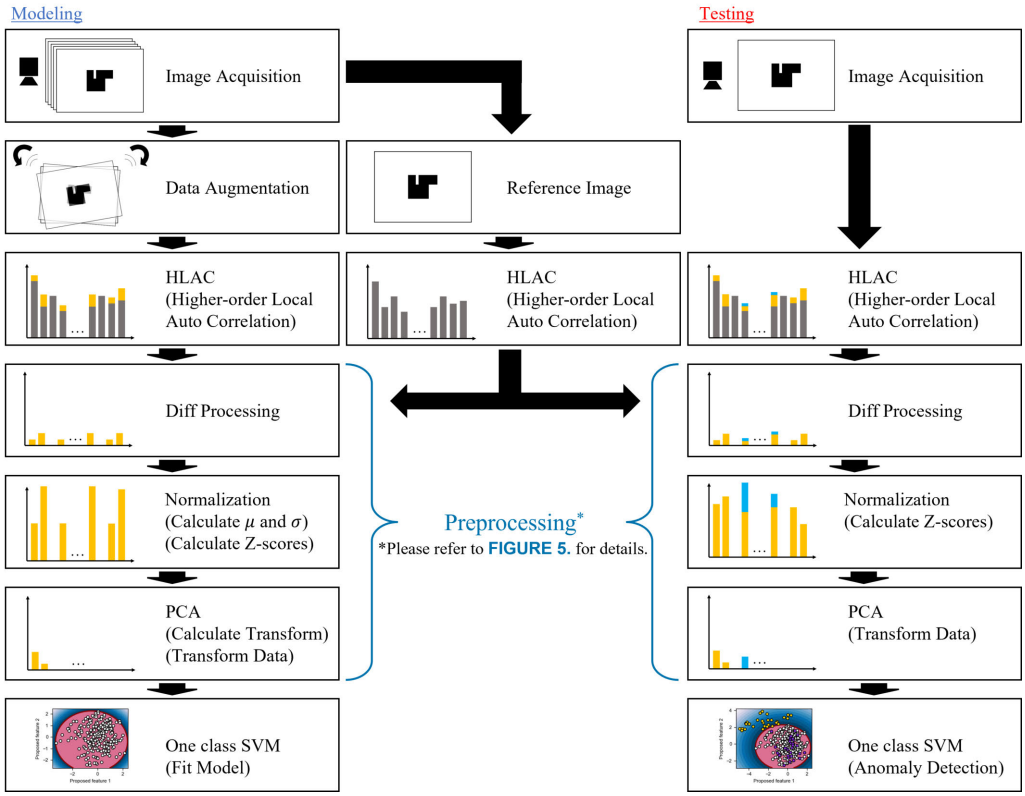

FIGURE 3. Flow of visual inspection.

B. INSPECTION PRINCIPLE

Fig. 3 shows the outline of the algorithm. The processing is divided into two phases: modeling and testing.

1) MODELING

In the modeling phase, the features of conforming parts are extracted and modeled using HLAC. Specifically, the HLAC features of the conforming sample is first calculated from a captured image of the reference plastic part. It is noted that the first sample is carefully set to the measuring place so that there is no deviation and rotation of the sample. The HLAC features are calculated, and these features are used as the reference. The HLAC is defined as a following Eq. (1). Considering a N^{th}-order autocorrelation with a set of displacements $\{a_1, \ldots, a_N\}$, the value of a feature H is obtained through the following function:

$$H(r, \{a_1, \ldots, a_N\}) = \int f(r) f(r + a_1) \ldots f(r + a_N)\, dr \quad (1)$$

Here, $f(r)$ corresponds to a list of intensity values of the pixels forming the processed image r. Based on the equation, the HLAC features are calculated as the integral of the local autocorrelation in the image.

The local patterns used are shown in the Fig. 4. In this study, we consider up to the second-order shift patterns. 35-dimensional features are obtained excluding the equivalent patterns.

As described in Section II-A, this research assumes that the target part will be roughly placed on the inspection place by human hands and the room brightness can be changed slightly due to accidental conditions. Because the captured image is affected by these inspection conditions, a large dataset with all the potential variations would typically be needed.

However, in our proposed system, only a small number of real samples are required. The influence of ambient light is reduced by maximizing the illumination intensity of the lighting illuminating the target part and the exposure time of the camera parameters. In addition, a number of images of conforming parts are taken to respond to minute changes in brightness that occur in this environment. To account for orientation variations, these images are augmented by random rotations to create a large number of artificial samples. Positional variations were not required because it does not affect HLAC features due to its shift-invariant property.

Next, the difference between the HLAC features of the conforming parts and that of the reference image is calculated. The means and standard deviations of these differences for these HLAC features are then calculated and the z-score normalization was performed for each HLAC feature. Even though HLAC features vary with rough alignment and slight brightness changes, many elements in the feature are highly correlated with each other. Therefore, a principal component

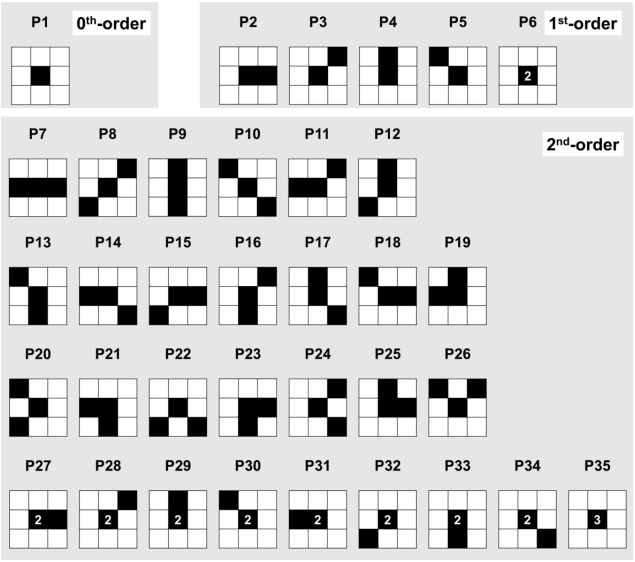

FIGURE 4. Local pattern for HLAC (Higher-order Local AutoCorrelation) feature.

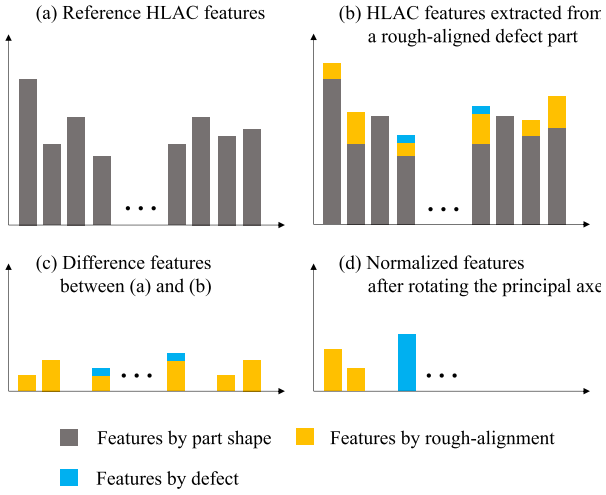

FIGURE 5. Concept diagram of the preprocessing.

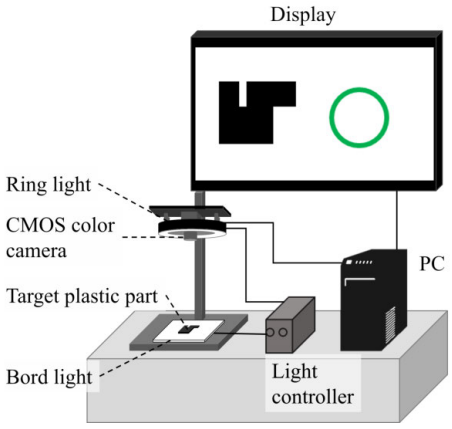

FIGURE 6. System components.

analysis is performed to obtain the eigenvectors. Using the obtained eigenvector matrix, each factor can be uncorrelated, and orientation information and anomalous information can be separated into different component. Each PCA component is then once again z-score normalized based on the means and standard deviations for that PCA component of the training data. A one-class SVM model is then trained using these normalized principal components calculated from only conforming parts. No nonconforming parts are used to train the model.

2) TESTING

In the testing phase, an image of target part is captured and the HLAC features are extracted from it. Then, the difference between the HLAC features of target part and that of the reference part is calculated. This difference features are then normalized and then transformed using the PCA eigenvector matrix derived in modeling phase. After obtaining the principal components, the features are further normalized based on the mean and standard deviation of the PCA components in the modeling data. Then, the one-class SVM model trained in the modelling section is used to detect nonconforming samples.

The concept diagram of the preprocessing is shown in Fig. 5. (a) Reference HLAC features, (b) HLAC features extracted from a rough-aligned nonconforming part, (c) difference features, (d) Normalized features after PCA transformation are shown. The gray bars indicate the HLAC features that reflect the shape of the plastic part, and they occupy most of the feature components. On the other hand, the yellow bars show the changes in features due to rough-alignment, and the blue bars show the changes in features due to defects such as underfill, burr, and etc. The yellow and blue bar can be extracted as the difference between the anomalous and reference features. However, the yellow bars are highly correlated. So, their principal axes are transformed with the eigenvector matrix, and each factor is uncorrelated and compressed into a few principal components. After normalizing the features based on the mean and standard deviation of the modeling data, anomalous feature is emphasized as shown in (d).

III. SYSTEM COMPONENTS

Fig. 6 shows an overview of the experimental system. As shown in the picture, the defect inspection is performed in a tabletop environment. A ring light (manufactured by Aitec System Co., Ltd., TR50 × 18-16WD-4) and a Board light (MUTOH INDUSTRIES LTD., SLT-B4C) are installed in the system. A CMOS color camera (manufactured by Logicool Co Ltd., C270) is used to capture images of the sample.

The CMOS color camera has a resolution of 720p and frame rate of 30[fps], the maximum view range is 55°, and the minimum focal length is 300[mm]. The brightness of the board illumination is about 2,700[lx]. The target

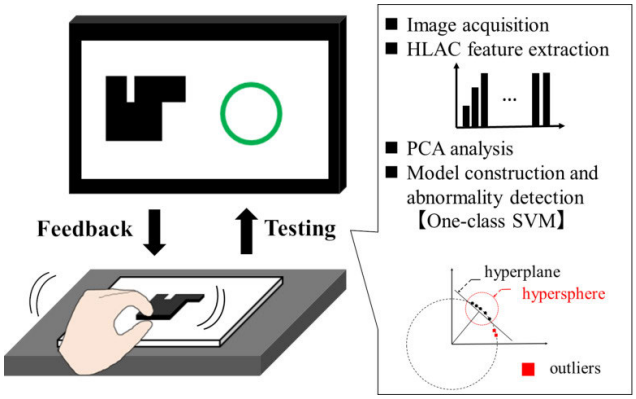

FIGURE 7. Software design.

plastic part can be roughly placed directly under the camera within the range of 80[mm] × 80[mm]. The distance between the camera and the target part is 300[mm]. The CMOS camera is connected to the computer via a USB interface.

The software configuration is shown in Fig. 7. The algorithm consists of four parts: image acquisition, HLAC feature extraction, PCA analysis, and model construction and defect detection. From image measurement is implemented using LabVIEW development environment (version 2018, National Instruments Corporation), and to PCA analysis to model construction of one-class SVM and defect detection are coded with Python program (version 3.8, Python Software Foundation). LabVIEW excels at building user interfaces to handle hardware control and data visualization. As for the development in Python, we adopt Scikit-learn module (version 1.0.2, Python Software Foundation) [22], which is capable for a machine learning.

The automatic parameter adjustment function of the CMOS camera is not used, and exposure time, gain, and focus is fixed at 0.8[sec], 0, 300[mm]. The images are continuously processes on the computer at the camera's frame rate of 30[Hz]. The images are first acquired as 32bit color image, and are then converted to a 8bit grayscale images. The brightness and contrast are adjusted in order to observe features of the plastic part in detail. As described in Section II-B, before the testing, the model has to be trained with conforming samples. 30 images of the same reference sample were captured all at once and these were augmented by randomly rotating them from −5 to 5 degrees to artificially generate 215 additional artificial samples.

HLAC features, we consider up to the second-order shift patterns. 35-dimensional features are obtained excluding the equivalent patterns. The HLAC features extracted from a conforming plastic part contains two linearly combined components. One is the feature derived from the shape of the part, and the other is derived from the measurement conditions such as part orientation light brightness, and etc.

The component components of the characteristic caused by the measurement conditions can be extracted by subtracting the reference characteristics of the conforming part. Each element of 35-dimensional vector is normalized $N(0, 1)$ based on the mean and standard deviation. In the 35-dimensional features, factors such as orientation, brightness, etc. are highly correlated each other. Therefore, PCA analysis is performed to uncorrelated each factor, and the changes in features due to rotation, brightness, etc. are aggregated into several principal components. After performing PCA, each element is normalized $N(0, 1)$ again based on the mean and standard deviation. The above calculation is not complicated and can be processed at high speed. The algorithm is implemented using LabVIEW, and the preprocessed features can be graphically observed on the monitor in real time.

The calculated 35-dimensional feature vectors are used for modeling/testing with one-class SVM. One-class SVM is a method that applies support vector machine (SVM) to one-class classification without supervised learning, which is a classification algorithm for machine learning [16]. In the method, all conforming samples are set to Cluster 1, and samples are mapped to a high-dimensional feature space based on the technique called Kernel trick so that only the origin of the feature space belongs to the anomalous cluster. Thus, the conforming samples are mapped far from the origin, and nonconforming samples are mapped near the origin. By training one-class SVM with only the conforming samples, the outlier sample can be detected based on the discrimination boundary. Even though almost no defect occurs and hardly any nonconforming samples are available, the anomaly detection can be performed. It is the remarkable feature of one-class SVM. The defining equations for a one-class SVM are Eq. (2)-(4), where α is a relative variable. K represents the kernel function and x_i, x_j are arbitrary features. Anomaly detection is performed based on Eq. (2). n represents the number of conforming sample data, and ν is a hyperparameter that determines the percentage of training errors. $f(x_i) \geq 0$ indicates conformity, and $f(x_i) < 0$ indicates anomaly.

$$f(x_i) = \min_{\alpha \in \mathbb{R}^n} \frac{1}{2} \sum_{i \in [n]} \sum_{j \in [n]} \alpha_i \alpha_j K(x_i, x_j) \tag{2}$$

$$s.t. \quad 0 \leq \alpha_i \leq \frac{1}{n\nu}, \forall i \in [n] \tag{3}$$

$$\sum_{i \in [n]} \alpha_i = 1 \tag{4}$$

The radial basis function (RBF) function was used for the kernel of one-class SVM. The RBF function is defined by Eq. (5). The hypersphere boundary of the model is generated based on Eq (5). Here x represents a feature. γ is a hyperparameter.

$$K(x_i, x_j) = exp(-\gamma ||x_i - x_j||) \tag{5}$$

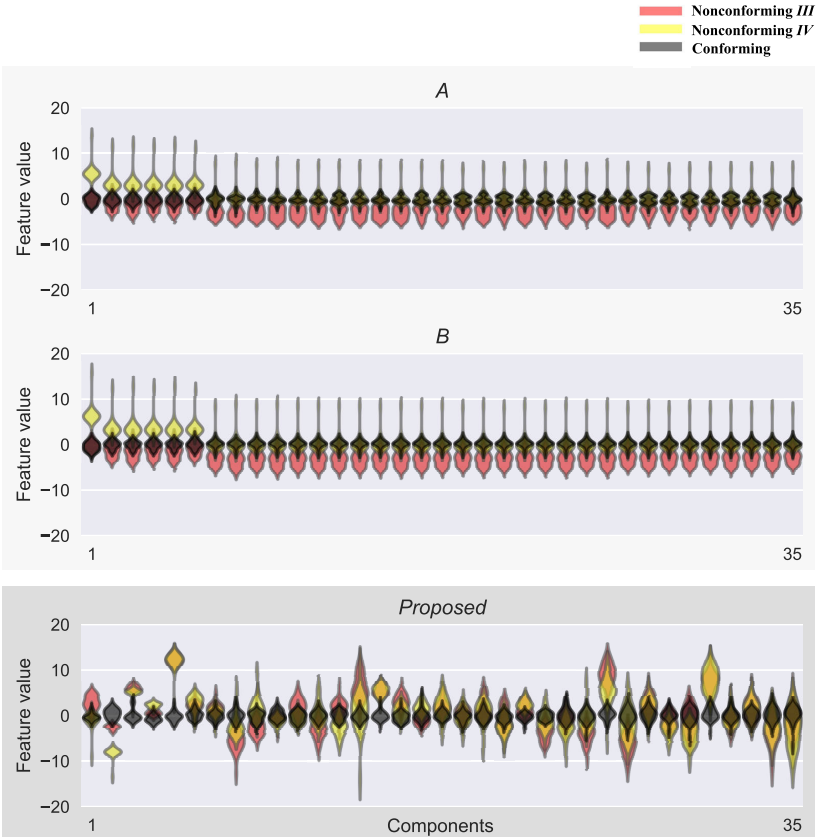

FIGURE 8. Violin plots showing the distribution of the original and preprocessed samples.

TABLE 1. Data set profile.

	Number of samples
Conforming (Model/Training)	245
Conforming (Test)	30
Nonconforming *I*	30
Nonconforming *II*	30
Nonconforming *III*	30
Nonconforming *IV*	30
Nonconforming *V*	30
Nonconforming *VI*	30

The parameter ν, which determines the ratio of outliers, was set to 0.02. Python program (version 3.8, Python Software Foundation) and Scikit-learn machine learning module (version 1.0.2, Python Software Foundation) was used to implement the algorithm of one-class SVM.

IV. EXPERIMENTS

An experiment was conducted to verify the validity and usefulness of the proposed method. This section introduces the experimental conditions and results.

A. EXPERIMENTAL CONDITIONS

Fig. 9 shows the conforming and nonconforming samples made to simulate manufacturing defects. The samples were made of black acrylic resin and the nonconforming parts were made by imitating actual defects commonly found in the plastic molded parts. Six types of nonconforming samples, *I* to *VI*, were used to simulate the typical defects found in injection molding. For nonconforming samples *III* and *IV*, the differences were enlarged to better highlight

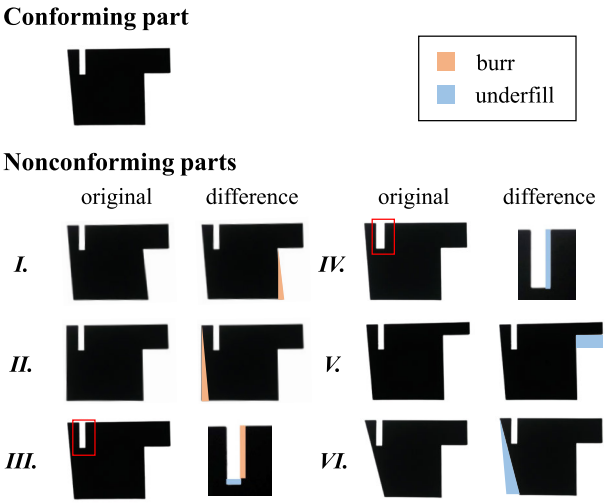

FIGURE 9. Conforming and nonconforming samples highlighting simulated manufacturing defects.

TABLE 2. Comparison of inspection accuracy based on number of dimensions.

Feature Name	Number of Dimension	TP *1	TN *2	FP *3	FN *4	Recall *5	Specificity *6
A	35	**1.00**	0.75	0.00	0.25	**1.00**	0.80
	10	0.97	0.80	0.03	0.20	0.97	0.83
	8	0.97	0.80	0.03	0.20	0.97	0.83
	5	0.93	0.96	0.07	0.04	0.93	0.96
	2	0.96	0.79	0.03	0.21	0.97	0.82
B	35	0.97	1.00	0.03	0.00	0.97	**1.00**
	10	**1.00**	**1.00**	0.00	0.00	**1.00**	**1.00**
	8	0.97	0.99	0.03	0.01	0.97	0.99
	5	0.97	0.90	0.03	0.10	0.97	0.91
	2	0.97	0.77	0.03	0.23	0.97	0.81
Proposed	31	0.43	**1.00**	0.57	0.00	0.43	**1.00**
	10	0.73	**1.00**	0.23	0.00	0.73	**1.00**
	8	0.77	**1.00**	0.23	0.00	0.77	**1.00**
	5	0.93	**1.00**	0.07	0.00	0.93	**1.00**
	2	**1.00**	**1.00**	0.00	0.00	**1.00**	**1.00**

*1 True Positive(TP): Percentage of conforming products determined to be conforming.
*2 True Negative(TN): Percentage of nonconforming products determined to be non-conforming.
*3 False Positive(FP): Percentage of nonconforming products determined to be conforming.
*4 False Negative(FN): Percentage of conforming products determined to be nonconforming.
*5 Recall: Percentage of conforming products correctly determined to be conforming. The definition formula is $TP/(TP + FN)$.
*6 Specificity: Percentage of nonconforming products correctly determined to be nonconforming. The definition formula is $TN/(TN + FP)$.
Red Number High accuracy value

the defective areas. Parts *I* and *II* simulated burr defects caused by overfilling, while parts *IV*, *V*, and *VI* simulated poor filling defects caused by insufficient filling. Finally, part *III* simulated both filling and burr defects simultaneously.

The data set used for modeling/testing is shown in Table 1. 245 conforming images were artificially augmented based on some images of the conforming part taken using the CMOS camera. The image was augmented by randomly rotated within the range of -5 to $+5$ degrees.

These 245 images of conforming parts were used for training of one-class SVM. Images of 30 conforming parts and 30 of each type of nonconforming parts *I* to *VI* were captured to be used for testing. While capturing the test image, the parts were repeatedly placed roughly by human hands, similar to the actual expected operation of the system.

B. VALIDITY OF THE PROPOSED ALGORITHM

To evaluate the effectiveness our algorithm, the proposed preprocessing and discriminator are compared with two other basic preprocessing procedures (A, B) and a discriminator (Elliptic Envelope). Thirty samples each of conforming, nonconforming *III*, and nonconforming *IV* (90 samples in total) were used for this validation testing. Fig. 8 shows violin plots of the features computed using two basic preprocessing procedures *A* and *B* as well as that for the proposed preprocessing. *A* in Fig. 8 shows the distribution of HLAC features without any processing while *B* in Fig. 8 shows the distribution of the difference in HLAC features between the test samples and the reference sample. *Proposed* in Fig. 8 shows the distribution of the features computed using the proposed method. The larger variance of the violin plots observed in *Proposed* in Fig. 8 shows the effect of the proposed preprocessing method to feature separation. It is difficult to feature separation because the defects in nonconforming parts *III* and *IV* are small, with only 1[mm] difference between them and the references sample. In addition, it is often difficult to identify nonconforming part *III* because multiple defects are mixed together. However, as shown in Fig. 8, the proposed method is even able to make the features of these nonconforming parts distinct.

The proposed discriminator was verified by comparing its accuracy for the three types of preprocessed features shown in Fig. 8 (*A*, *B*, and *Proposed*) with that of Elliptic Envelope. The boundary condition parameters of the Elliptic Envelope and the one-class SVM are determined by trial and error for each feature. Table 2 shows the One-class SVM accuracy for each feature when the number of dimensions is reduced. The confusion matrices showing True Positive (TP), True Negative (TN), False Positive (FP), and False Negative (FN) percentages are reported and the recall, specificity ratios are shown for each feature and selected number of dimensions. The proposed method is always able detect nonconforming products because specificity does not decrease with a change in the number of dimensions. In other words, the proposed method can achieve the same inspection performance for a small number of dimensions as it does for a high number of dimensions. Based on the above, the results of the comparison in five dimensions are shown in Table 3. For each feature, it shows the percentage of conforming and nonconforming samples identified. The results in Table 3 confirm that the proposed method can detect anomalies that could not be detected by no prepossessing. For comparison, anomaly detection using Elliptic Envelope was performed on the same data set as in Table 3. Table 4 shows the discrimination results using Elliptic Envelope. As shown in Table 3, the method using one-class SVM performed better for *A* and *B*. Therefore, we decided to use 5-dimensional features in our subsequent experiments. In addition, to confirm the appearance of the boundaries in each feature, two features were selected from the lower dimensions and illustrated in Fig. 10. For comparison, the same dataset as in Fig. 10 was

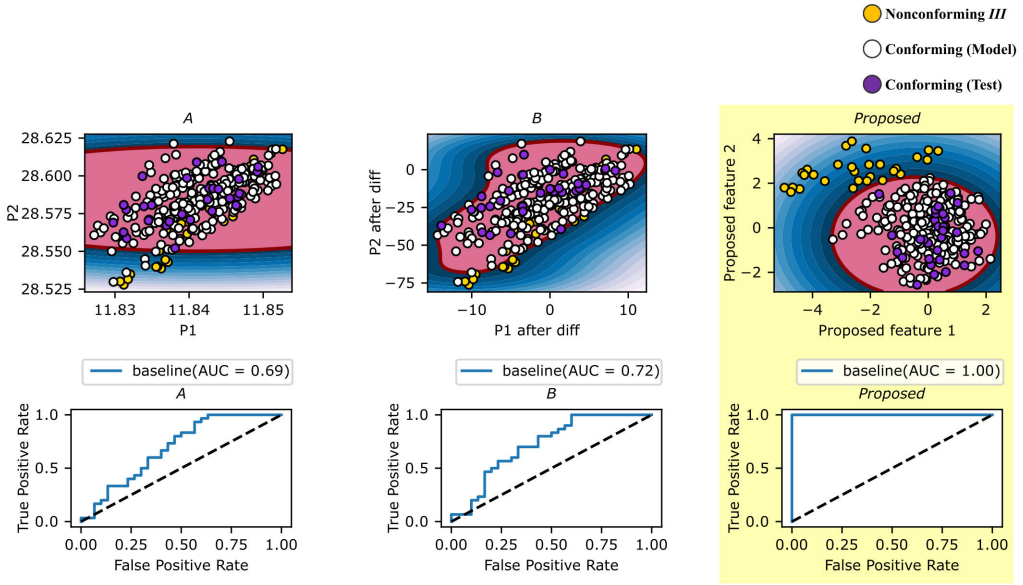

FIGURE 10. Boundary visualization by 2D distribution(One-class SVM).

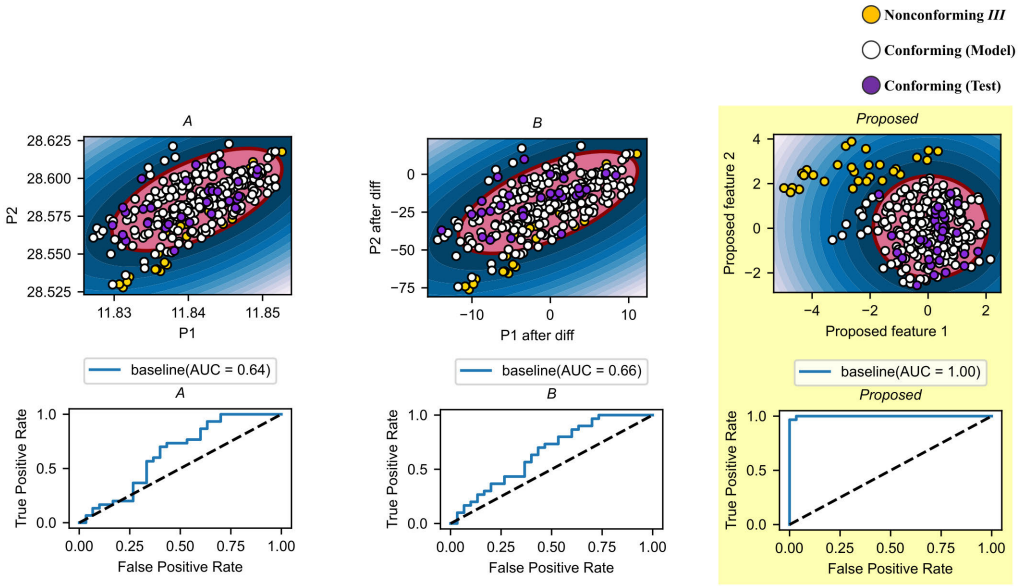

FIGURE 11. Boundary visualization by 2D distribution (Elliptic Envelope).

used to test for anomaly detection using the Elliptic Envelope. The results are shown in Fig. 11. As shown in Fig. 10, the method using one-class SVM shows that the discriminant curve is better fitted to the distribution in B. The ROC curve in Fig. 10 also shows that the performance is better when one-class SVM is used.

C. PRACTICAL CHALLENGE

Finally, an experiment was conducted to prove the effectiveness of the method in practical operation. A total of 300 samples (270 samples for conforming parts and 5 samples for each of the 6 types of nonconforming parts *I* -*VI*] were prepared. Three conditions were investigated, namely, (a) visual inspection by human operators and (b) automated inspection requiring precise alignment, and (c) defect inspection by the proposed system. In (b), the inspection is performed by specifying the position of the parts in detail and requiring the participant to align them manually. In (c), the inspection is performed with rough alignment, where the part is allowed to be placed roughly in the inspection area, taking advantage of the features of the proposed method.

TABLE 3. Comparison of discriminator (one-class SVM) performance for *A*, *B* and *Proposed* preprocessing procedures (5 PCA-dimensions).

		A		B		Proposed	
		Conforming	Nonconforming	Conforming	Nonconforming	Conforming	Nonconforming
Modeling	Conforming	0.96	0.40	0.98	0.02	0.91	0.09
	Nonconforming	-	-	-	-	-	-
Testing	Conforming	0.93	0.07	0.97	0.03	0.93	0.07
	Nonconforming *I*	0.00	**1.00**	0.00	**1.00**	0.00	**1.00**
	Nonconforming *II*	0.00	**1.00**	0.00	**1.00**	0.00	**1.00**
	Nonconforming *III*	0.23	0.77	0.60	0.40	0.00	**1.00**
	Nonconforming *IV*	0.00	**1.00**	0.00	**1.00**	0.00	**1.00**
	Nonconforming *V*	0.00	**1.00**	0.00	**1.00**	0.00	**1.00**
	Nonconforming *VI*	0.00	**1.00**	0.00	**1.00**	0.00	**1.00**

Red Number High accuracy value

TABLE 4. Comparison of discriminator (Elliptic Envelope) performance for *A*, *B* and *Proposed* preprocessing procedures (5 PCA-dimensions).

		A		B		Proposed	
		Conforming	Nonconforming	Conforming	Nonconforming	Conforming	Nonconforming
Modeling	Conforming	0.90	0.10	0.90	0.10	0.90	0.10
	Nonconforming	-	-	-	-	-	-
Testing	Conforming	0.93	0.07	0.90	0.10	0.93	0.07
	Nonconforming *I*	0.00	**1.00**	0.00	**1.00**	0.00	**1.00**
	Nonconforming *II*	0.00	**1.00**	0.00	**1.00**	0.00	**1.00**
	Nonconforming *III*	**0.63**	**0.37**	**0.63**	**0.37**	0.00	**1.00**
	Nonconforming *IV*	0.00	**1.00**	0.00	**1.00**	0.00	**1.00**
	Nonconforming *V*	0.00	**1.00**	0.00	**1.00**	0.00	**1.00**
	Nonconforming *VI*	0.00	**1.00**	0.00	**1.00**	0.00	**1.00**

Red Number High accuracy value
Blue Number Lower value than One-class SVM

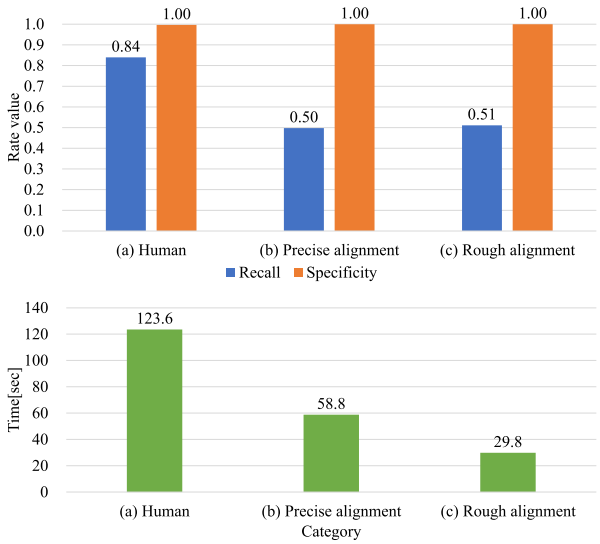

FIGURE 12. The results of the comparison are practical challenges.

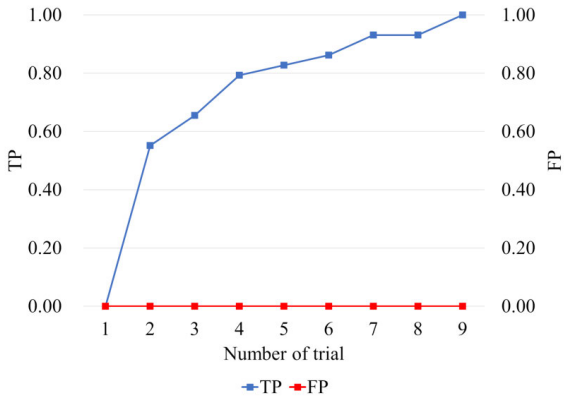

FIGURE 13. Repetitive True Positive.

The results of the experiment are shown in Fig. 12.(a), (b), and (c) correspond to the respective inspection conditions. It was observed that (c) the proposed system (rough alignment) was the fastest and (a) human visual inspection was the slowest. There is a four-fold difference in efficiency between (c) and (a). The difference between (b) and (c) is the accumulated difference in time spent aligning the parts; On average, alignment of the inspection parts takes an extra of 30[sec].

Recall, an indicator of false positive detection of conforming products, was inferior to that of the proposed system compared to human inspection. However, Table 3 shows that the proposed system does not mistake any nonconforming product for a conforming product. The false positive detection of conforming products is caused by problems with slight changes in brightness and timing of image capture. Therefore, it may be possible to reduce the false positive rate of conforming products by repeating the inspections of those deemed nonconforming. Based on this, we prepared 30 conforming products that were judged to be nonconforming and one each of kind of six nonconforming products. If a product is determined to be conforming at least once during repeated inspections, it is considered to be conforming. Fig. 13 shows the results. The results show that all of the conforming products were correctly judged as conforming in nine trials in this experiment. These FP values also indicate that nonconforming products were always judged as nonconforming in the nine trials. In other words, repeated inspections are effective in solving the problems of this system.

V. CONCLUSION

The paper validates the effectiveness of rough alignment for rapid and interactive anomaly inspection in a manufacturing line. We demonstrated that a system using HLAC features with PCA and pretreatment maximizes the benefits of the features and clarified its effectiveness.

In this research, an automatic defect inspection system was developed to meet the needs of the practical manufacturing site. The system can detect nonconforming parts with high accuracy in an extremely short time, helping human operator inspect various types of parts in small quantities while maintaining extremely high quality of products. The developed system does not require accurate alignment of the target parts, so it has the advantage of reducing the work load on the human operator.

The method proposed in this paper has the following novelties and usefulness. As a novelty, the proposed method provides robust anomaly detection in rough alignment. HLAC feature has the outstanding feature of being feature-invariant with respect to parallel shifts of the target. However, it has been extremely difficult to detect anomalies with high accuracy from rough-aligned (e.g., rotating) objects. The proposed method solves this problem by effectively combining HLAC, computation of differences, PCA, and one-class SVM. Another academic contribution is the example of detecting anomalies such as burrs and chips of less than 1[mm]. The usefulness of this system lies in the fact that it can be quickly applied to manufacturing sites using only inexpensive cameras, and that it can extract only the necessary feature components without compromising the characteristics of the HLAC features. We conducted experiments using samples to verify the validity and usefulness of the proposed algorithm.

The experimental results showed that defects can be detected with high efficiency and high accuracy. In the future, we would like to extend the developed abnormality inspection system based on 3D data using a depth camera. We would also like to try to introduce deep learning techniques into the classifier to improve detection accuracy.

REFERENCES

[1] T. S. Newman and A. K. Jain, "A survey of automated visual inspection," *Comput. Vis. Image Understand.*, vol. 61, no. 2, pp. 231–262, Mar. 1995, doi: 10.1006/cviu.1995.1017.

[2] D.-M. Tsai and T.-Y. Huang, "Automated surface inspection for statistical textures," *Image Vis. Comput.*, vol. 21, no. 4, pp. 307–323, 2003, doi: 10.1016/S0262-8856(03)00007-6.

[3] J. Deng, W. Dong, R. Socher, L.-J. Li, K. Li, and L. Fei-Fei, "ImageNet: A large-scale hierarchical image database," in *Proc. IEEE Conf. Comput. Vis. Pattern Recognit.*, Jun. 2009, pp. 248–255.

[4] R. Waseem and Z. Wang, "Deep convolutional neural networks for image classification: A comprehensive review," *Neural Comput.*, vol. 29, no. 9, pp. 2352–2449, Sep. 2017, doi: 10.1016/S0262-8856(03)00007-6.

[5] J. Redmon, "You only look once: Unified, real-time object detection," *Neural Comput.*, vol. 29, no. 9, pp. 2352–2449, 2016, doi: 10.1162/neco_a_00990.

[6] M. Abnishek, "Amazon Rekognition," in *Machine Learning in the AWS Cloud: Add Intelligence to Applications With Amazon SageMaker and Amazon Rekognition*. Hoboken, NJ, USA: Wiley, Sep. 2019, pp. 421–444.

[7] N. Otsu and T. Kurita, "A new scheme for practical, flexible and intelligent vision systems," in *Proc. IAPR Workshop Comput. Vis.*, 1988, pp. 431–435.

[8] E. Hu, H. Nosato, H. Sakanashi, and M. Murakawa, "Anomaly detection for capsule endoscopy images using higher-order local auto correlation features," in *Proc. IEEE Int. Conf. Syst., Man, Cybern. (SMC)*, Oct. 2012, pp. 2289–2293, doi: 10.1109/ICSMC.2012.6378082.

[9] Y. Mitani, R. B. Fisher, Y. Fujita, Y. Hamamoto, and I. Sakaida, "Image correction methods for regions of interest in liver cirrhosis classification on CNNs," *Sensors*, vol. 22, no. 9, p. 3378, Apr. 2022, doi: 10.3390/s22093378.

[10] Y. Hatanaka, "Automated blood vessel extraction using local features on retinal images," in *Proc. SPIE*, vol. 9785, pp. 626–632, Mar. 2016, doi: 10.1117/12.2216572.

[11] T. Kobayashi and N. Otsu, "Action and simultaneous multiple-person identification using cubic higher-order local auto-correlation," in *Proc. 17th Int. Conf. Pattern Recognit. (ICPR)*, vol. 4, 2004, pp. 741–744, doi: 10.1109/ICPR.2004.1333879.

[12] B. Lin, "Hotspot classification based on higher-order local autocorrelation," *Proc. SPIE*, vol. 8522, vol. 8522, pp. 705–714, Nov. 2012, doi: 10.1117/12.964384.

[13] H. Nosato, H. Sakanashi, E. Takahashi, M. Murakawa, T. Matsunawa, S. Maeda, S. Tanaka, and S. Mimotogi, "Hotspot prevention and detection method using an image-recognition technique based on higher-order local autocorrelation," *J. Micro/Nanolithography, (MEMS, MOEMS)*, vol. 13, no. 1, Feb. 2014, Art. no. 011007.

[14] K. Uehara, H. Sakanashi, H. Nosato, M. Murakawa, H. Miyamoto, and R. Nakamura, "Object detection of satellite images using multi-channel higher-order local autocorrelation," in *Proc. IEEE Int. Conf. Syst., Man, Cybern. (SMC)*, Oct. 2017, pp. 1339–1344, doi: 10.1109/SMC.2017.8122799.

[15] V. Vapnik and A. Lerner, "Pattern recognition using generalized portrait method," *Automat. Remote Control*, vol. 24, pp. 774–780, May 1963.

[16] B. Schölkopf, J. C. Platt, J. C. Shawe-Taylor, A. J. Smola, and R. C. Williamson, "Estimating the support of a high-dimensional distribution," *Neural Comput.*, vol. 13, no. 7, pp. 1443–1471, 2001, doi: 10.1162/089976601750264965.

[17] F. T. Liu, K. M. Ting, and Z.-H. Zhou, "Isolation forest," in *Proc. 8th IEEE Int. Conf. Data Mining*, Dec. 2008, pp. 413–422, doi: 10.1109/ICDM.2008.17.

[18] F. T. Liu, K. M. Ting, and Z. Zhou, "Isolation-based anomaly detection," *ACM Trans. Knowl. Discovery From Data*, vol. 6, no. 1, pp. 1–39, Mar. 2012, doi: 10.1145/2133360.2133363.

[19] M. M. Breunig, H.-P. Kriegel, R. T. Ng, and J. Sander, "LOF: Identifying density-based local outliers," in *Proc. ACM SIGMOD Int. Conf. Manage. Data*, May 2000, pp. 93–104, doi: 10.1145/342009.335388.

[20] P. J. Rousseeuw and K. Van Driessen, "A fast algorithm for the minimum covariance determinant estimator," *Technometrics*, vol. 41, no. 3, pp. 212–223, Aug. 1999.

[21] K. Pearson, "LIII. On lines and planes of closest fit to systems of points in space," *London, Edinburgh, Dublin Phil. Mag. J. Sci.*, vol. 2, no. 11, pp. 559–572, Jun. 2010, doi: 10.1080/14786440109462720.

[22] F. Pedregosa, "Scikit-learn: Machine learning in Python," *J. Mach. Learn. Res.*, vol. 12 no. 10, pp. 2825–2830, 2012.

TAIGA EGUCHI received the B.E. degree from the Faculty of Science and Engineering, Saga University, Japan, in 2021, where he is currently pursuing the degree with the Department of Information Science.

His current research interest includes image processing.

WEN LIANG YEOH received the M.Eng. degree in mechanical engineering from Imperial College London, U.K., in 2013, and the Ph.D. degree from Kyushu University, Japan, in 2020. Since 2022, he has been a Project Assistant Professor with the Faculty of Science and Engineering, Saga University, Japan. His research interests include gait assistance, motor control, and human–robot cooperation. He is a member of the Japan Human Factors and Ergonomics Society.

HIROSHI OKUMURA received the B.E. and M.E. degrees from Hosei University, Tokyo, Japan, in 1988 and 1990, respectively, and the Ph.D. degree from Chiba University, Chiba, Japan, in 1993.

He is currently a full Professor with the Graduate School of Science and Engineering, Saga University, Japan. His current research interests include remote sensing and image processing. He is a member of the International Society for Optics and Photonics (SPIE), the Institute of Electronics, Information and Communication Engineers (IEICE), and the Society of Instrument and Control Engineers (SICE).

NOBUHIKO YAMAGUCHI received the Ph.D. degree in intelligence and computer science from the Nagoya Institute of Technology, Japan, in 2003.

He is currently an Associate Professor with the Faculty of Science and Engineering, Saga University. His research interest includes neural networks. He is a member of the Japan Society for Fuzzy Theory and Intelligent Informatics.

OSAMU FUKUDA (Member, IEEE) received the B.E. degree in mechanical engineering from the Kyushu Institute of Technology, Iizuka, Japan, in 1993, and the M.E. and Ph.D. degrees in information engineering from Hiroshima University, Higashihiroshima, Japan, in 1997 and 2000, respectively.

In 2000, he joined the Mechanical Engineering Laboratory, Agency of Industrial Science and Technology, Ministry of International Trade and Industry, Japan. From 2001 to 2013, he was a member of the National Institute of Advanced Industrial Science and Technology, Japan. Since 2014, he has been a Professor with the Graduate School of Science and Engineering, Saga University, Japan. He is currently a Guest Researcher with the National Institute of Advanced Industrial Science and Technology, Japan. His current research interests include human interface and neural networks.

Dr. Fukuda is a member of the Society of Instrument and Control Engineers, Japan. From 1997 to 1999, he was a Research Fellow with the Japan Society for the Promotion of Science. He received the K. S. Fu Memorial Best Transactions Paper Award from the IEEE Robotics and Automation Society, in 2003.